AD-A108 686 SCIENCE APPLICATIONS INC MCLEAN VA F/G 8/3
MODELS OF NEAR INERTIAL VERTICAL SHEAR,(U)
NOV 81 D M RUBENSTEIN N00014-81-C-0084
UNCLASSIFIED SAI-82-546-WA NL

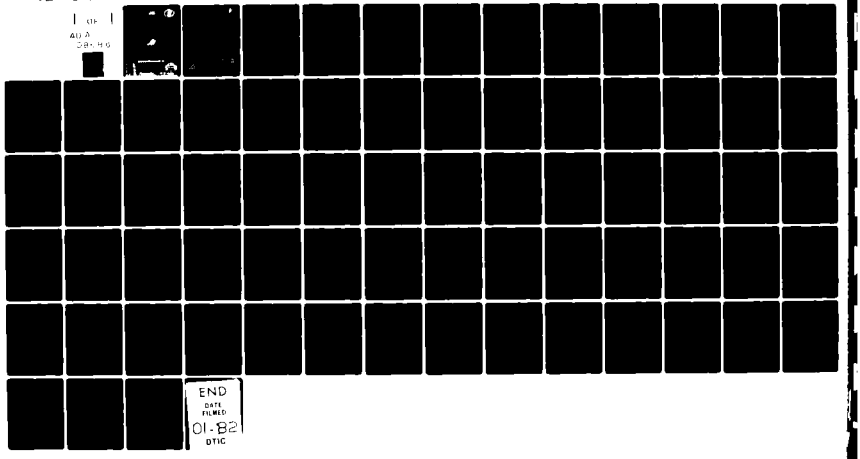

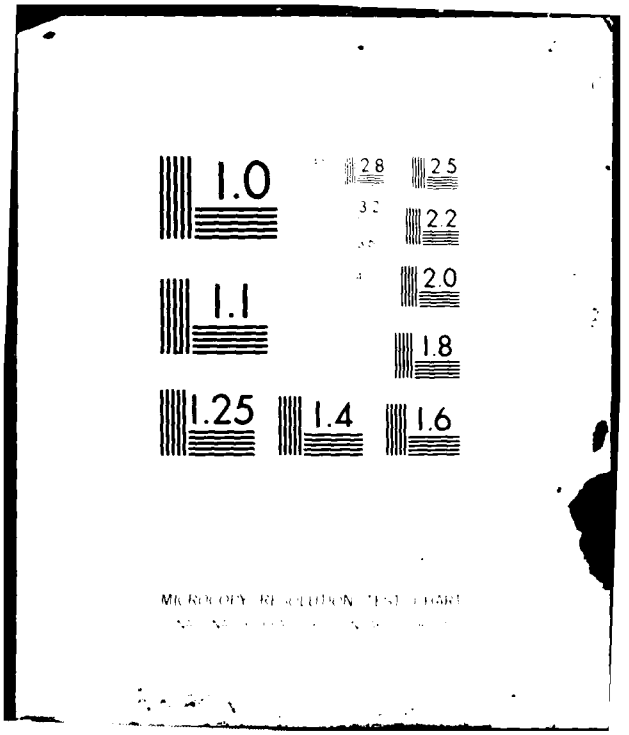
1.0
2.8
2.5
3.2
2.2
2.0
1.1
1.8
1.25
1.4
1.6

MODELS OF NEAR INERTIAL VERTICAL SHEAR

SAI-82-546-WA

Accession For	
NTIS GRA&I	X
DTIC TAB	☐
Unannounced	☐
Justification	
By	
Distribution/	
Availability Codes	
Dist	Avail and/or Special
A	

ATLANTA • ANN ARBOR • BOSTON • CHICAGO • CLEVELAND • DENVER • HUNTSVILLE • LA JOLLA
LITTLE ROCK • LOS ANGELES • SAN FRANCISCO • SANTA BARBARA • TUCSON • WASHINGTON

MODELS OF NEAR INERTIAL VERTICAL SHEAR

SAI-82-546-WA

OPD-81-274-04

November 1981

Prepared by:
David Rubenstein

Prepared for:
Naval Ocean Research and Development Activity
NSTL Station, Mississippi 39529

Prepared Under Contract No. N00014-81-C-0084

SCIENCE APPLICATIONS, INC.
1710 Goodridge Drive
P.O. Box 1303
McLean, Virginia 22102
(703) 821-4300

UNCLASSIFIED

SECURITY CLASSIFICATION OF THIS PAGE (When Data Entered)

REPORT DOCUMENTATION PAGE	READ DISTRUCTIONS BEFORE COMPLETING FORM
1. REPORT NUMBER: SAI-82-546-WA	2. GOVT ACCESSION NO.: AD-A108 656
	3. RECIPIENT'S CATALOG NUMBER:
4. TITLE (and Subtitle): Models of Near Inertial Vertical Shear	5. TYPE OF REPORT & PERIOD COVERED:
	6. PERFORMING ORG. REPORT NUMBER: SAI-82-546-WA
7. AUTHOR(s): David M. Rubenstein	8. CONTRACT OR GRANT NUMBER(s): N00014-81-C-0084
9. PERFORMING ORGANIZATION NAME AND ADDRESS: Science Applications, Inc. 1710 Goodridge Drive P.O. Box 1303, McLean, VA 22102	10. PROGRAM ELEMENT, PROJECT, TASK AREA & WORK UNIT NUMBERS:
11. CONTROLLING OFFICE NAME AND ADDRESS: NORDA, Code 540 Ocean Measurements Program NSTL Station, Bay St. Louis, MS 39529	12. REPORT DATE: November, 1981
	13. NUMBER OF PAGES: 62
14. MONITORING AGENCY NAME & ADDRESS(if different from Controlling Office): SAME	15. SECURITY CLASS. (of this report): UNCLASSIFIED
	15a. DECLASSIFICATION/DOWNGRADING SCHEDULE:

16. DISTRIBUTION STATEMENT (of this Report)

Distribution unlimited; approved for public release

17. DISTRIBUTION STATEMENT (of the abstract entered in Block 20, if different from Report)

SAME

18. SUPPLEMENTARY NOTES

19. KEY WORDS (Continue on reverse side if necessary and identify by block number)

Inertial Oscillations
Ekman Layer
Internal Waves
Shear

20. ABSTRACT (Continue on reverse side if necessary and identify by block number)

The physics of the interactions between the wind stress, the Ekman layer, and internal waves are reviewed. A general set of equations which describe near-inertial motions are developed. The time dependent behavior of the wind-forced Ekman layer is examined. Then we consider two classes of resonance conditions. The first involves the resonance between the wind field and Ekman pumping, while the second class is the resonance between a propagating Ekman pumping field and the internal wave field.

DD FORM 1 JAN 73 1473 EDITION OF 1 NOV 65 IS OBSOLETE
S/N 0102-LF-014-6601

UNCLASSIFIED
SECURITY CLASSIFICATION OF THIS PAGE (When Data Entered)

TABLE OF CONTENTS

LIST OF FIGURES

Section 1
INTRODUCTION

1.1 BACKGROUND

Classical Ekman theory considers a steady wind stress acting over a homogeneous ocean of infinite depth and constant eddy viscosity. The surface current deflects 45° to the right of the wind direction (in the Northern Hemisphere), and the deflection angle increases with depth. The current magnitude is greatest at the surface and decreases exponentially with depth.

If the wind velocity were to change suddenly, the currents would evolve toward their new equilibrium profile. This approach to the new equilibrium would be oscillatory, with inertial frequency $f = 2\Omega\sin\phi$, where $\Omega = 2\pi/\text{day}$ is the rotation rate and ϕ is the latitude. These inertial oscillations can often be difficult to observe. Inertial oscillations are transient in nature, and can require long time series of current records to make identification. At latitudes where f coincides with tidal frequencies, inertial oscillations can be difficult to distinguish from tidal motions. Examples of these difficulties are shown in Webster (1968).

There are two components of the near-inertial wave field; a global and a local component. The global component is generated by a variety of mechanisms at lower latitudes as super-inertial internal waves. If these waves propagate away from the equator, they appear as inertial

waves when they reach their turning latitude. As they can reflect off the bottom and top ocean surfaces, and off irregularities in the Vaisala frequency profile, they may be observed to propagate upwards as well as downwards. Since these waves are observed in locations that are far from their geographical areas of generation, they probably can only be described in a statistical sense. Fu (1980) shows that the global component of the near-inertial wave field in the deep ocean (over smooth topography) can be described successfully with a universal spectral model.

There is also a local component of the near-inertial wave field. The strongest evidence that a component of the wave field is locally forced is the observation that the dominant direction of the phase propagation is upward. According to the internal wave dispersion relationship, this corresponds to downward energy propagation. The implication is that the surface layer of the ocean acts as a source for these waves. In brief, the hypothesized mechanism is as follows. When the wind stress field is inhomogeneous in space, a vertical velocity field, known as Ekman pumping, deforms the interface between the surface layer and the stratified interior. If these vertical motions are resonant with near-inertial internal waves, then energy can propagate away from the interface, into the deep interior.

The purpose of the present study is to investigate the locally forced component of the near-inertial internal wave field. In particular, we are interested in the propagation of near-inertial motions and vertical shear from the

surface layer into the upper ocean thermocline. It behooves us to separate the problem conceptually into two parts. In the first part we examine the generation of inertial oscillations in the surface layer. Much of the shear across the base of the wind-mixed layer is due to these inertial oscillations, and this shear is an important factor in the deepening of the mixed layer. Inertial shear across the mixed layer/thermocline interface gives rise to shear instabilities, which help to entrain water across the interface and erode the thermocline (Pollard et al., 1973; Kruass, 1981). Thus, the inertial oscillations in the mixed layer are important in their own right.

The second part of our problem is the transferral of near-inertial energy from the mixed layer into the thermocline. Near-inertial kinetic energy is not as strong here, but the background stratification in the thermocline allows the energy to propagate into the deeper waters, in the form of free internal gravity waves. These waves are excited through resonances between the wind field, Ekman pumping, and the internal wave field.

This report reviews the interactions between the wind stress, the Ekman layer, and internal waves in the interior. The purpose is not to relate an exhaustive list of the models, theories and observations of inertial motions. Instead, our purpose is to lay a basic foundation, with strong emphasis on the physical dynamics which underly inertial motions. In Section 1.2 we develop the general set of equations which describe near-inertial motions. In Section

2 we look into the time dependent response of the wind-forced Ekman layer. A number of different cases and conditions are examined. We show how the attenuation rate of inertial oscillations may be related (indirectly, through the eddy viscosity) to the background stratification. In Section 3 we explore two classes of resonance conditions. The first class involves the resonance between the wind field and the Ekman pumping. This sort of resonance is characterized by an oscillatory wind field whose frequency is in the neighborhood of f. The second class is the resonance between a propagating Ekman pumping field and the internal wave field. This resonance activates wave packets whose phase velocity is equal to the propagation speed. In Section 4 we discuss the role of future research in understanding inertial oscillations and vertical shear.

Wherever possible, we attempt to cast light on the structure of vertical shear. In our data analysis report (Rubenstein and Newman, 1981), we showed evidence that vertical shear may be a better indicator of near-inertial frequency oscillations than the current.

1.2 SCALING THE EQUATIONS OF MOTION

We wish to develop a set of equations that can be used to describe various aspects of near-inertial-frequency motions. We begin with the momentum equations for an incompressible fluid with negligible molecular viscosity

$$\rho D_t \underline{u} + 2\rho(\underline{\Omega} \times \underline{u}) = -\nabla P - \rho \underline{g} - \underline{F} , \qquad (1.1)$$

and the equations of mass conservation and continuity

$$D_t \rho = -\gamma \ , \quad \nabla \cdot \underline{u} = 0 \ . \tag{1.2a,b}$$

The symbols ρ and P denote density and pressure, $\underline{u} = (u,v,w)$ is the velocity vector, and $\underline{g}$ is gravitational acceleration. F and γ are the divergences of turbulence momentum flux and mass flux, respectively, due to unresolved motion. The symbol D_t denotes the substantive derivative $\partial_t + \underline{u} \cdot \nabla$, and $\underline{\Omega}$ is the local component of the earth's angular rotation vector. We define a coordinate system with z positive upwards; x and y are the conventional zonal and meridional directions. The mean ocean surface lies at z = 0, and the flat bottom at z = -H.

We are interested in the small fluctuating motions that perturb a stationary reference state. This reference state is defined by the stratification $\rho_r(z)$ which satisfies the hydrostatic relation

$$d_z P_r = -g\rho_r(z) \ . \tag{1.3}$$

The total density and pressure are given by

$$P(x,y,z,t) = P_r(z) + P'(x,y,z,t) \ ,$$

$$\rho(x,y,z,t) = \rho_r(z) + \rho'(x,y,z,t) \ , \tag{1.4a,b}$$

where P' and ρ' are perturbations from the reference state. We assume that these density perturbations are small;

$$\rho' \ll \rho_r \ ,$$

so we make the Boussinesq approximation, in which the effects of fluctuations in density on the momentum balance are neglected, except in the buoyancy term. We define buoyancy to be

$$b = -\frac{\rho'}{\rho_o} g \ , \tag{1.5}$$

where ρ_o is a representative value for the density. Then (1.1) and (1.2) become

$$D_t \underline{u} + 2(\underline{\Omega} \times \underline{u}) = -\frac{1}{\rho_o} \nabla P' + b\hat{z} - \underline{F}/\rho_o \tag{1.6}$$

$$D_t b + wN^2(z) = -B \ , \quad \nabla \cdot \underline{u} = 0 \ , \tag{1.7a,b}$$

where B is the divergence of buoyancy flux, $\hat{z}$ is the unit vector in the vertical direction, and N(z) is the buoyancy frequency defined by

$$N^2(z) = -\left(\frac{g}{\rho_o}\right)\left(\frac{d\rho_r}{dz}\right) \ . \tag{1.8}$$

These equations are too general for our purposes, so a number of assumptions allow suitable simplifications. We are interested in near-inertial period motions. The time scale of interest is $T = \pi/\Omega$. We assume that both $\underline{u}$ and ρ vary over the same horizontal length scale, L. This length scale is that over which appreciable variations occur in surface wind stress or surface buoyancy flux. We assume that the aspect ratio $\delta = H/L$ is very small; $\delta \sim O(10^{-2})$.

We nondimensionalize as follows;

$$
\begin{aligned}
(x,y) &= (x^*,y^*)L, \\
(u,v) &= (u^*,v^*)U, \\
z &= z^*H, \\
w &= w^*W, \\
t' &= t^* f_o^{-1}, \\
P' &= P^* P_o, \\
b &= b^* B_o, \\
N &= N^* N_o,
\end{aligned}
\qquad (1.9a\text{-}h)
$$

where asterisks indicate nondimensional quantities, $f_o = 2\Omega$, and N_o is a representative value of N(z). We substitute (1.9) into (1.7b) to obtain (dropping asterisks)

$$
\frac{U}{L}\,(u_x + v_y) + \frac{W}{H}\,w_z = 0 \qquad (1.10)
$$

If w_z is to be the same order of magnitude as the horizontal velocity divergence, then

$$
W = \delta U \; ; \qquad (1.11)
$$

the ratio of vertical to horizontal velocities is of the order of the aspect ratio or smaller.

Next we scale the buoyancy equation, (1.7a);

$$
\begin{aligned}
B_o b_t + \left(\frac{U}{f_o L}\right) B_o (u b_x + v b_y + w b_z) + \left(\frac{\delta U N_o^2}{f_o}\right) w N^2 \\
= -\left(\frac{u^* b^*}{f_o L}\right) \left[(\overline{u'b'})_x + (\overline{v'b'})_y + \delta^{-1}(\overline{w'b'})_z\right] .
\end{aligned}
\qquad (1.12)
$$

The overbars written over the buoyancy flux represent averages over the time scale f_o^{-1}. The primed quantities are the nondimensional buoyancy and velocity components that vary appreciably over time scales small compared to f_o^{-1}, and their dimensional magnitudes are b^* and u^*. We neglect the horizontal divergence terms of the buoyancy flux because they are of order δ smaller than the vertical divergence term. We are interested in small velocity perturbations, such that the Rossby number U/f_oL is much less than unity. We therefore neglect the nonlinear advection terms. We require that in the absence of small time scale fluctuations, b_t should be balanced by wN^2. Therefore, $B_o = \delta UN_o^2/f_o$, and (1.12) becomes

$$b_t + wN^2 = -\left(\frac{u^*b^*}{Hf_oB_o}\right)(\overline{w'b'})_z \quad . \tag{1.13}$$

We apply similar arguments to the horizontal momentum equation (1.6) to obtain

$$u_t - \sin\phi v = -P_x - \left(\frac{u^{*2}}{Hf_oU}\right)(\overline{u'w'})_z \quad ,$$

$$v_t + \sin\phi u = -P_y - \left(\frac{u^{*2}}{Hf_oU}\right)(\overline{v'w'})_z \quad , \tag{1.14a,b}$$

where terms of order δ and of order U/f_oL have been neglected, and $P_o = \rho_oUf_oL$ has been asserted.

The vertical momentum equation deserves special attention. We drop the nonlinear advection terms and the horizontal flux divergence terms to get

$$\delta^2 w_t - \delta \cos\phi v = -P_z + \left(\frac{\delta N_o}{f_o}\right)^2 b - \delta \left(\frac{u^{*2}}{Hf_o U}\right) (\overline{w'w'})_z \quad . \tag{1.15}$$

We define $N_o = f_o/\delta$; then the balance is hydrostatic;

$$0 = -P_z + b \quad . \tag{1.16}$$

The vertical momentum flux divergence is of order $\delta(u^{*2}/Hf_oU)$ with respect to the pressure gradient P_z, while the horizontal flux divergence terms in (1.14) are of order (u^{*2}/Hf_oU). Thus, the vertical flux divergence in (1.15) is neglected. We also drop the w_t and $\cos\phi v$ terms, because they are of order δ^2 and δ. Nearly all investigators drop the $\cos\phi v$ term, the so called "traditional approximation", but sometimes the w_t term is retained. It is necessary to retain this term for the case of high frequency motions, where $T \ll f_o^{-1}$. But (1.15) shows that for near-intertial-frequency motions, the nonstationary term should be dropped, and it is inconsistent to retain w_t without also retaining the vertical Coriolis force term, $\cos\phi v$. A number of investigators make this mistake, and we wish to point out this inconsistency.

Having determined which terms we wish to retain, we list below the dimensional equations of motion for easy reference;

$$u_t - f_o \sin\phi v = -p_x - (\overline{u'w'})_z$$

$$v_t + f_o \sin\phi u = -p_y - (\overline{v'w'})_z$$

$$0 = -p_z + b$$

$$b_t + wN^2(z) = -(\overline{w'b'})_z$$

$$u_x + v_y + w_z = 0 \quad , \qquad (1.17a\text{-}e)$$

where $p = P'/\rho_o$ has been substituted, to simplify the appearance of (1.17).

Section 2
THE EKMAN LAYER

In this section we review the transient behavior of inertial motions in a surface layer. We begin though, with a brief discussion of the steady state balance between the Coriolis force and vertical stress, the classical Ekman spiral. Then we discuss the sudden onset of surface stress over an initially quiescent ocean; horizontal currents accelerate, oscillate at near-inertial frequencies, and asymptotically approach the Ekman spiral velocity profile.

In the way we formulate momentum diffusion, the stratification enters our problem only indirectly, through the eddy viscosity parameter. We note in Section 2.4, that a constant eddy viscosity may be most appropriate in a continuously stratified ocean, where the scale of momentum-transferring eddies is not a function of depth. In a homogeneous surface layer the stress is nearly constant, and the eddy viscosity might be better described as a linear function of depth. This model leads to better agreement with observations of attenuation rates of inertial oscillations. We conclude this section with a discussion of the situation where an unstratified mixed layer terminates in a density interface, and overlies a stable diffusion-free layer. We briefly describe how shear across the interface controls the entrainment rate which, in turn, by its control of the mixed layer depth, influences the character of shear in the Ekman layer.

The equations of motion used in this section are developed as follows. Consider a horizontally homogeneous unstratified ocean, at latitude ϕ, with constant eddy viscosity K. Equations (1.17) reduce to

$$u_t - fv - Ku_{zz} = 0$$

$$v_t + fu - Kv_{zz} = 0 \quad , \qquad (2.1a,b)$$

where $f = 2\Omega\sin\phi$ is the Coriolis parameter. The boundary conditions are

$$K\underline{u}_z = \hat{\underline{\tau}}_o(t) \qquad z = 0 \quad ,$$

$$\underline{u} \to 0 \qquad z \to -\infty \quad , \qquad (2.1c,d)$$

where $\hat{\underline{\tau}}_o$ is an imposed surface stress vector.

We define a complex velocity $U = u + iv$, so that (2.1) can be combined to read

$$U_t + ifU - KU_{zz} = 0 \quad ,$$

$$KU_z = \tau_o(t) \qquad z = 0 \quad ,$$

$$U \to 0 \qquad z \to -\infty \quad , \qquad (2.2a\text{-}c)$$

where τ_o is the complex surface stress.

2.1 THE EKMAN SPIRAL

Before considering the solution to this problem, we first examine the steady state situation, where the

Coriolis force is balanced by friction in the ocean interior. This problem is easily solved by setting U_t in (2.2) equal to zero. A method of solution is derived in Appendix A. We rewrite the solution (A.10) in a more convenient, easily recognizable form;

$$u(z) = V_o \exp(-\pi|z|/D)\cos(\pi/4 - \pi|z|/D)$$

$$v(z) = V_o \exp(-\pi|z|/D)\sin(\pi/4 - \pi|z|/D). \quad (2.3a,b)$$

Here a surface stress is applied in the y-direction, V_o is the magnitude of the surface current, and the Ekman depth is given by

$$D = \pi(2K/f)^{1/2} . \quad (2.4)$$

Figure 2.1 shows the Ekman spiral, and we note that at the surface, the direction of the current is 45° to the right (clockwise) of the wind. If we integrate (A.10) from $z = -\infty$ to ∞, then the resultant vector is

$$R_o = \int_{-\infty}^{\infty} U(z)dz = -i\sqrt{2}\tau_o/f \quad . \quad (2.5)$$

This result states that the total mass transport in a water column is rotated 90° clockwise with respect to the direction of the surface stress vector.

It is also of interest to note that the shear, defined by $S = (u_z^2 + v_z^2)^{1/2}$, can be computed from (2.3);

$$S = \frac{\sqrt{2}\pi V_o}{D} \exp(-\pi|z|/D) \quad . \quad (2.6)$$

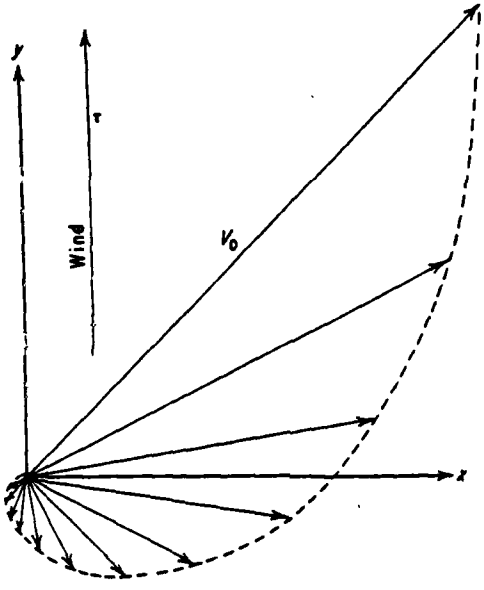

Figure 2.1 Ekman spiral for pure wind-driven currents projected on a horizontal plane. V_0 is the surface velocity vector deviated by 45° to the right of the wind vector (Northern Hemisphere). [After Ekman (1905).]

The shear is simply an exponentially decaying function of depth, with an e-folding length scale D/π.

2.2 TIME DEPENDENT SOLUTION - INERTIAL TRANSIENTS

We return now to the time dependent problem, described by equation (2.2). We adapt Gonella's (1971) method to our present needs by considering three cases; I) an initial velocity $U_o(z) = U(z,0)$ and vanishing surface stress $\tau_o(t) = 0$, II) a surface stress $\tau_o(t) = \tau(0,t)$ and vanishing initial velocity $U_o(z) = 0$, and III) surface stress lasts for a finite duration. We outline our method of solution in Appendix A. The general solution is the sum of cases I and II;

$$U(z,t) = U_1(z,t) \underset{(z)}{*} U_o(z) + U_1(z,t) \underset{(t)}{*} 2\tau_o(t) \ ,$$

where

$$U_1(z,t) = Y(t) \frac{e^{-ift}}{(4\pi Kt)^{1/2}} \exp(-z^2/4Kt) \ , \qquad (2.7)$$

and $Y(t)$ is the Heaviside step function. The asterisks denote convolution operations, the first with respect to z and the second with respect to t.

2.2.1 Case I: Initial Velocity Profile

When the initial complex velocity $U_o(z) = U(z,0)$ is nonzero, and the stress $\tau_o(t)$ is set equal to zero, then the first part of (2.7) is the solution for $U(z,t)$. For large t, the solution asymptotically approaches

$$U(z,t) \to \frac{e^{-ift}}{(4\pi Kt)^{1/2}} R_o \exp(-z^2/4Kt) \ , \qquad (2.8)$$

where $R_o = R(t = 0)$ is the initial resultant vector defined by

$$R(t) = \int_{-\infty}^{\infty} U(z,t)\, dz \quad . \tag{2.9}$$

This result, as pointed out by Gonella, shows that the velocity asymptotically becomes independent of z, as t becomes very large. The amplitude decays as $t^{-1/2}$, and the limiting period is $2\pi/f$, the inertial period. The current at each level tends to come into phase with the resultant of the initial distribution, R_o. At a given depth z, depending on whether $U_o(z)$ leads or lags with respect to R_o, the period theoretically tends to the inertial period from above or from below (see Figure 2.2). Gonella claims that this effect might to some extent be responsible for observations of spectral peaks being distributed in the vicinity of the inertial frequency; f $\pm$ 2 to 4%. According to (2.3), an initial angular difference of $\pi/2$ between $U_o(z)$ and R_o becomes zero after about ten inertial periods, and gives an average period of $2\pi/f \pm 2.5\%$.

For the situation where a constant stress suddenly shuts off at t=0, then we have, in effect, a case where the initial velocity $U_o(z)$ is the Ekman spiral (2.3). We showed, in equation (2.5), that the initial resultant vector R_o is rotated 90° to the right of the wind direction. From (2.3), the depth z at which $U_o(z)$ is rotated 90° to the right of the wind is -D/4. For a typical value of eddy viscosity K = 100 cm^2/sec, the value of D at midlatitudes is on the order of 50 m. If the steady wind stress were to terminate suddenly, then the asymptotic evolution of the current profile for large t approaches that given by (2.4).

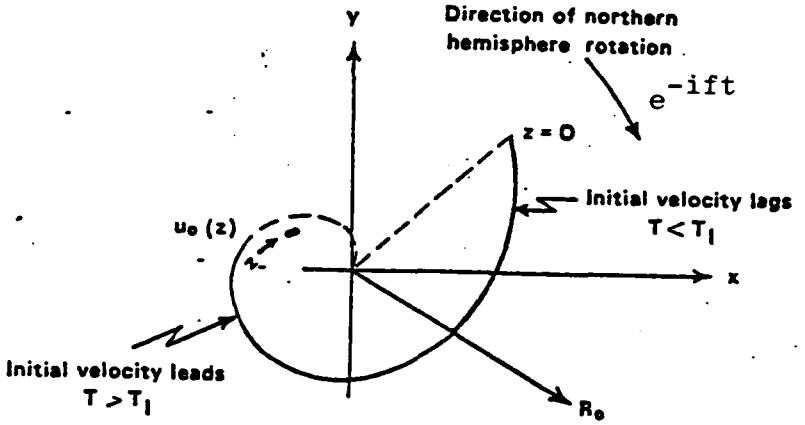

Figure 2.2 Initial velocity distribution, $u_0(z)$. If the initial velocity is either leading or lagging the resultant velocity R_0, it will tend to come into phase with R_0 through the action of viscosity. Note that the period is less ($T < Ti$) for that part of the distribution which lags and is greater ($T > Ti$) for that part which leads. From Gonella (1971).

At depths shallower than D/4, about 12.5 m, the velocity vector should begin to rotate with a frequency greater than the inertial frequency, while at depths deeper than D/4, the rotation should be at a lower frequency.

Kundu (1976) computed high resolution kinetic energy spectra from current meter observations taken in shallow water (100 m deep) off the Oregon coast. In order to achieve statistical stability, he ensemble averaged spectra from eleven depths ranging from 3.4 to 95.9 m. Figure 2.3 shows two spectral peaks, one above and one below the inertial frequency. Although the unstratified, laterally unbounded, infinitely deep ocean model does not directly apply to these observations, Figure 2.3 is suggestive of the theoretical mechanism being described here.

2.2.2 Case II: Surface Stress

When the constant surface stress τ_o is turned on at t = 0 over an ocean initially at rest, the solution for U(z,t) is given by the second part of (2.7). Performing the convolution with respect to t, the solution is

$$U(z,t) = 2\tau_o \int_0^t \frac{e^{-if\theta}}{(4\pi K\theta)^{1/2}} \exp(-z^2/4K\theta)\, d\theta \quad . \qquad (2.10)$$

This is Fredholm's solution for the response after a sudden onset of wind stress. Figure 2.4 shows this solution as a function of time, at the surface and at depths z = -.5D, -D, and -2D, where D is the Ekman depth. The tick marks along

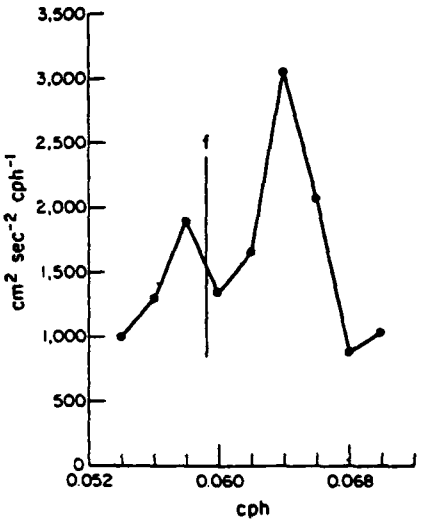

Figure 2.3 High-resolution spectra of KE (= $u^2 + v^2$), averaged over all eleven depths. Bandwidth = 0.002 cph. Note the shift of the inertial peak to 0.064 cph, and the secondary peak at 0.058 cph. From Kundu (1976).

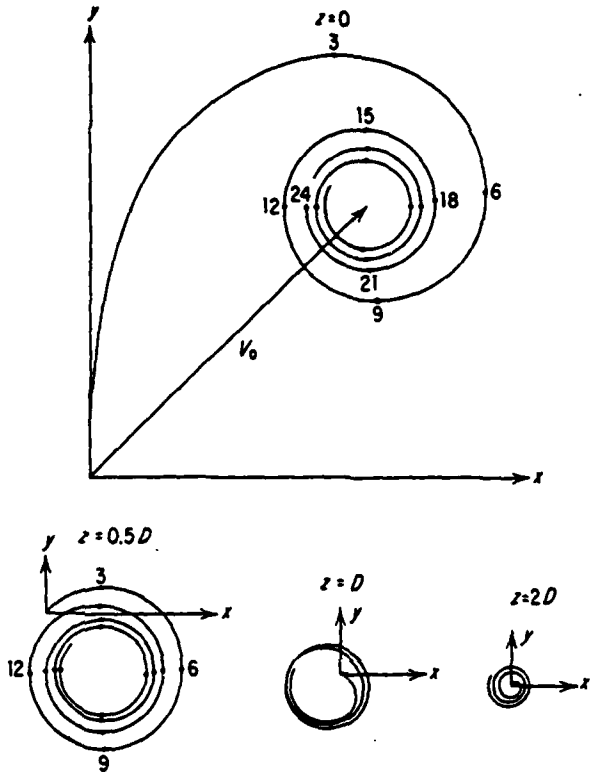

Figure 2.4 Hodographs showing the development of a pure drift current (infinitely deep ocean) with time at different depths. The depth, z, is given in terms of the thickness of the upper layer of frictional influence, D, and the time in pendulum hours after the start of a constant wind. [After Ekman (1905).]

the spirals indicate periodic time intervals, and are labeled in units of pendulum hours. The current vectors rotate around the steady state current vector, and asymptotically approach the Ekman spiral solution (2.3).

2.2.3 Case III: Surface Stress for a Finite Duration

When an initially quiescent ocean is suddenly driven by a surface stress that lasts for a duration d, we might approach the problem by giving the wind stress the form

$$\tau_o(t) = \underline{\tau}_o\left[Y(t) - Y(t-d)\right] \quad , \tag{2.11}$$

where Y is the Heaviside step function. We substitute (2.11) into the second part of (2.7) to get

$$U(z,t) = 2\tau_o \int_{t-d}^{t} \exp(-z^2/4K\theta)\, \frac{e^{-if\theta}}{(4\pi K\theta)^{1/2}}\, d\theta \quad . \tag{2.12}$$

An asymptotic expansion of (2.12) as $t \to \infty$ may be written

$$U(z,t) \to \frac{2\tau_o e^{-i\pi/2}}{f(4\pi Kt)^{1/2}} \left(1 - e^{-ifd}\right) e^{-ift} \quad . \tag{2.13}$$

As in case I, the period approaches the inertial period, and the amplitude decays as $t^{-1/2}$. The term $(1 - e^{-ifd})$ acts as an amplification factor. If the duration d is an integer multiple n of the inertial period ($d = 2\pi n/f$), then this factor vanishes, and the oscillations decay rapidly after

the wind terminates. If the duration is a half-integer multiple of the inertial period, $d = 2\pi(n+1/2)/f$, then the amplification factor is maximized.

An instantaneous change in the wind stress contains Fourier components at all frequencies. The deeper water, though, is shielded from stress changes on small time scales. At some depth z, stress changes are communicated on a time scale of order z^2/K. This suggests that in a time dependent Ekman layer, motions are in the angular frequency range $f \pm \Delta f$, where $\Delta f \leq K/z^2$. If current measurements show energy outside this frequency range, then these motions are due to phenomena other than diffusive penetration of surface stress changes.

2.3 COMPARISON WITH OBSERVATIONS

Gonella (1971) compared selected aspects of the time dependent solution, described in Section 2.2, with current measurements taken in the Mediterranean Sea. Three periods of observations corresponded to times when the atmospheric conditions were favorable for comparisons with theoretical results. During each of these periods, a relatively long period of calm weather followed storms which could be well modeled by an impulsive rectangle, conforming to Case III.

Preceding two of these measurement periods, the average winds were of comparable intensity, about 14 m/sec, but lasted different durations. Currents measured during July 1964 at 20 m depth were about twice as strong as those during July 1968 at 10 m depth. The first measurements were taken after a storm event that lasted for 1½ inertial

periods, while the latter measurements followed a storm event that lasted 2 inertial periods. As discussed in Section 2.2.3, the asymptotic response approached long after termination of the wind is maximum for wind events lasting half-integer multiples of the inertial period, and vanishes for integer multiple durations. The observations are consistent with this model result.

Figure 2.5 shows the attenuation of inertial oscillations during the three observational periods. In each case, the attenuation rate was greater than the theoretical $t^{-1/2}$ rate. Gonella finds the observed attenuation rate to be related to surface layer stratification. During the July 1964 and 1968 measurements, the stratification was continuous down to 30-35 m. The anomalous attenuation rate during December 1964 was measured in a surface layer that was homogeneous down to about 70 m. We refer the reader to Section 2.4 for a possible explanation of this anomaly.

2.4 DEPTH-DEPENDENT EDDY VISCOSITY

Gonella (1971) made a cogent comment concerning Ekman layer models. He noted that although the Ekman's model was developed for a homogeneous ocean, the assumption of a uniform eddy viscosity is more realistic in a continuously stratified ocean. There is a hint in Figure 2.5, that Gonella's model may be better applied in a stratified rather than in an unstratified surface layer.

Madsen (1977) addresses this issue by solving the Ekman layer problem with a depth dependent eddy viscosity. He starts with a generalization of equation (2.2);

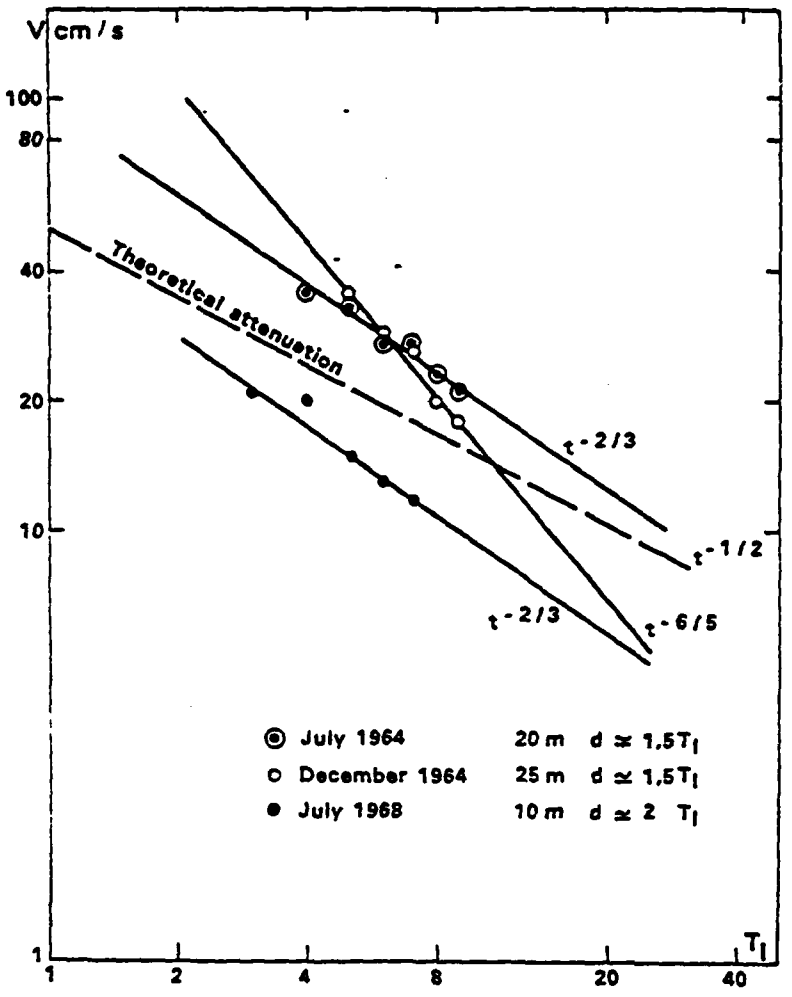

Figure 2.5: Attenuation of inertial currents as a function of time. The time origin has been chosen as the beginning of the wind stress, and the time is expressed in units of inertial period. From Gonella (1971). During July 1964 and 1968, the stratification was continuous down to 30-35m. During December 1964, the surface layer was homogeneous down to 70m.

$$U_t + ifU = \left[K(z)U_z\right]_z \ , \tag{2.14}$$

where $U = u + iv$ is the complex horizontal velocity vector. A linear form

$$K(z) = \kappa u_* |z| \tag{2.15}$$

is assumed for the eddy viscosity, which is presumed to be appropriate in a homogeneous surface layer. Here $\kappa = 0.4$ is von Karman's constant and $u_* = (|\tau_o|/\rho)^{1/2}$ is a friction velocity based on a representative value of surface stress magnitude $|\tau_o|$. The boundary conditions, as in Section 2.1 and 2.2, are that stress be continuous at the surface, and that $U \to 0$ as $z \to -\infty$. The general solution for an initially quiescent ocean is of the form

$$U(z,t) = \frac{\tau_o(t)}{\kappa u_*} \underset{(t)}{*} \frac{e^{-ift}}{t} \exp(-|z|/\kappa u_* t) \ , \tag{2.16}$$

where the asterisk denotes a *convolution* with respect to t. This solution is of a form analogous to (2.7) for the uniform eddy viscosity, but we call the reader's attention to an important difference. The asymptotic time dependence here, with the depth dependent eddy viscosity, is proportional to t^{-1}, whereas (2.7) has a $t^{-1/2}$ proportionality. Referring to Figure 2.5, we see that Madsen's model better predicts the attenuation rate for the December 1964 data set. If we suppose that additional processes besides turbulent mixing are simultaneously contributing to the attenuation of inertial currents, then we conclude that the models and data are consistent: In a neutrally stratified surface layer, inertial currents decay with a rate at least

as fast as t^{-1}, and in a stably stratified surface layer, the decay rate is at least as fast as $t^{-1/2}$. An example of an additional process which could contribute to attenuation is internal gravity wave dispersion, discussed in Section 4 of this report.

Madsen illustrates that his model is different from the constant eddy viscosity model in other respects. Figure 2.6 compares the vertical profile of velocity in hodograph form with the classical Ekman spiral. Two important differences appear. First, the deflection angle between surface wind stress and surface current is much smaller, about 10°, as opposed to 45° for the Ekman spiral. Madsen points out that his result is consistent with observations of oil spill trajectories, both real and simulated, which show deflection angles of order 10° or less. Second, there is a more rapid decrease and rotation of the current vector with depth. The vertical shear of the steady state current, in the limit of small depth ($z \ll u_*/f$) is

$$S = (u_z^2 + v_z^2)^{1/2} \simeq \frac{u_*}{\kappa |z|} \quad . \tag{2.17}$$

Unlike the exponential decay of the Ekman spiral in (2.6), the shear in the depth dependent eddy viscosity model is approximately inversely proportional to depth. The shear at $z = 0$ in (2.17) is infinite, a result of the fact that since $K(z)$ vanishes at $z = 0$, (2.16) is a divergent integral at the surface. Madsen copes with this problem by translating the vertical coordinate by a distance $k_s/30$, where k_s is a typical value of surface roughness, about 4 cm for moderate (3-10 m/sec) surface wind speeds.

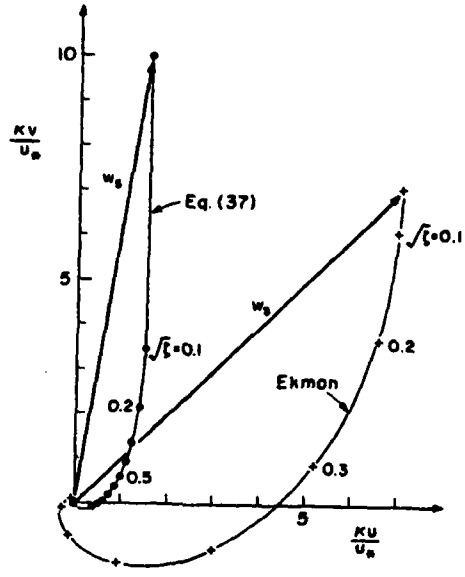

Figure 2.6: Vertical velocity structure of a pure drift current in an infinitely deep homogeneous ocean of infinite lateral extent, comparing the turbulent Ekman spiral (•) and the classical Ekman spiral (+). From Madsen (1977).

The temporal evolution of the depth-dependent eddy viscosity model is much more rapid than Fredholm's solution (2.10). Figure 2.7 compares the buildup of the surface current after the sudden onset of surface stress. The time increments are labeled in pendulum hours. A pendulum hour is equal to a sidereal hour divided by the sine of the latitude. A requirement that surface current magnitudes be equal was imposed on the solutions. The solution to Madsen's model approaches a steady state within about three pendulum hours. The reason for the faster adjustment rate is that the equivalent value of eddy viscosity, evaluated at $z = -u*/2f$, is about 50 times the value in the classical, constant eddy viscosity model.

2.5 DENSITY INTERFACE LIMITED EKMAN LAYER

So far we have discussed the behavior of an Ekman layer in a homogeneous, infinitely deep ocean. With a sudden change in surface stress, a momentum impulse diffuses downward. The leading edge of such an impulse lies at a depth of order $(2Kt)^{1/2}$. After a while, the Coriolis force leads to a cross flow which soon balances the stress. As a result of this balance, most of the vertical shear is confined within the Ekman depth, $D = \pi(2K/f)^{1/2}$.

When a mixed layer of depth h lies above a stably stratified layer, where turbulent diffusion is suppressed by the buoyancy force, the vertical growth of the surface shear layer is stopped. Csanady and Shaw (1980) developed a model that describes the interaction between these two depth limiting mechanisms. They suppose that entrainment of fluid

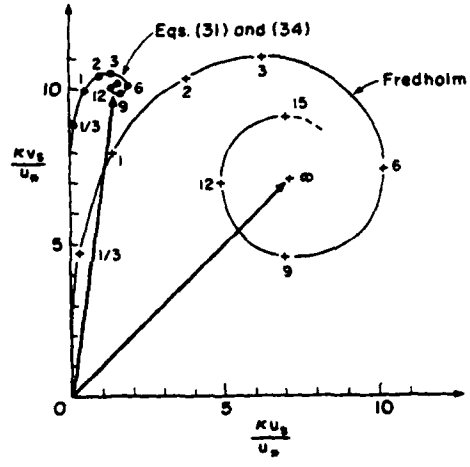

Figure 2.7: The temporal development of the surface drift current due to a suddenly applied uniform surface shear stress. Time from time of application is indicated in pendulum hours. The present eddy viscosity model is shown by solid circles and Fredholm's classical solution by plus signs. From Madsen (1977).

from the stable layer, across the density gradient interface, into the mixed layer can be related to the stress at the interface. If the velocity in the stable layer just below the interface is zero, then the interface stress may be written in terms of the eddy viscosity:

$$K\underline{u}_z = c_d\underline{u}(u^2+v^2)^{1/2} \quad \text{at } z = -h \quad . \tag{2.18}$$

where c_d is a drag coefficient.

The entrainment velocity w_e is presumably proportional to some power of the interfacial friction velocity

$$u_{**} = \left[c_d(u^2+v^2) \right]^{1/2} \quad , \tag{2.19}$$

and is consequently proportional to the magnitude of the shear Δu across the interface. Csanady and Shaw choose a power law found by Csanady (1978);

$$\frac{w_e}{u_{**}} = 0.004 \left(\frac{u_{**}^3}{\nu g \Delta\rho/\rho} \right)^{1/2} \tag{2.20}$$

where τ is kinematic viscosity and $\Delta\rho$ is the density jump across the interface.

After an initial momentum impulse reaches the mixed layer depth, entrainment begins. As the mixed layer depth increases, the interface shear Δu decreases, and the entrainment rate also decreases. If the mixed layer depth is much greater than the Ekman depth (h>>D), then negligible velocities at $z = -h$ give rise to no further entrainment.

It seems likely that an initially shallow mixed layer depth should asymptotically approach a small multiple of the Ekman depth.

Csanady and Shaw (1980) numerically integrated equations (2.1) but rather than using the boundary condition (2.1d) that velocity vanish at infinity, they imposed the boundary condition (2.18). The surface stress was taken to be in the y-direction, and the initial value for h was 9 m. A uniform eddy viscosity was parameterized as

$$K = u_* h/R \ , \qquad (2.21)$$

where u_* was the surface friction velocity and R = 12 was a Reynolds number. Sample solutions are shown in Figures 2.8 and 2.9. At any given depth, the velocity is a superposition of a constant component plus an inertially oscillating component. When the components at the mixed layer bottom are in phase, the entrainment rate quickens. The inertially oscillating component damps more quickly in Figure 2.9 because the initial mixed layer depth is shallower.

Csanady and Shaw also note that in Figure 2.9, where the ratio h/D is quite small, the velocity component u (perpendicular to the wind) is nearly uniform in the mixed layer, approximately u_*^2/fh. The implication is that the interior stress varies almost linearly from a maximum at the surface, to zero at the interface. The wind stress is distributed almost evenly across the mixed layer and balanced by the Coriolis force of a nearly constant drift to the right of the wind.

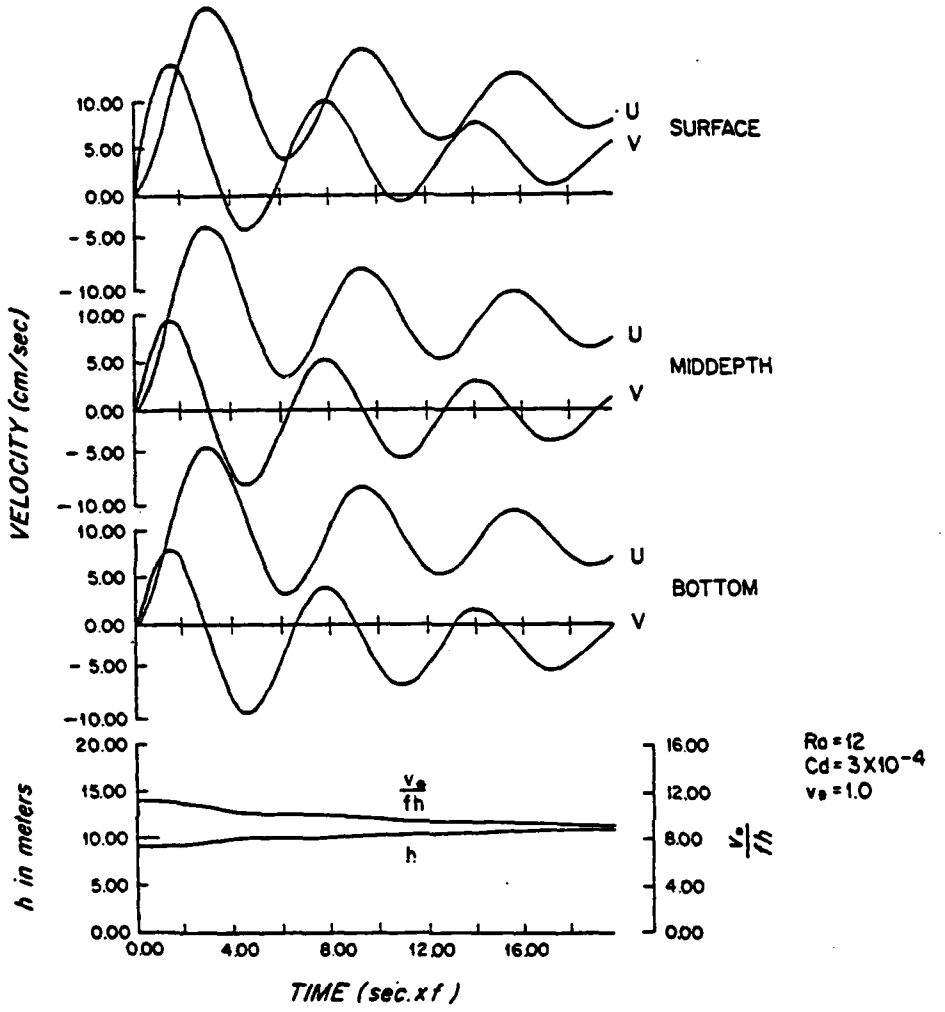

Figure 2.8: Evolution of velocity components u, v, depth h, and $\alpha (= v_*/f/h)$ as a function of time from numerical solutions with R = 12, $c_d = 3 \times 10^{-4}$, $v_* = 1$, and initial depth 9m. From Csanady and Shaw (1980).

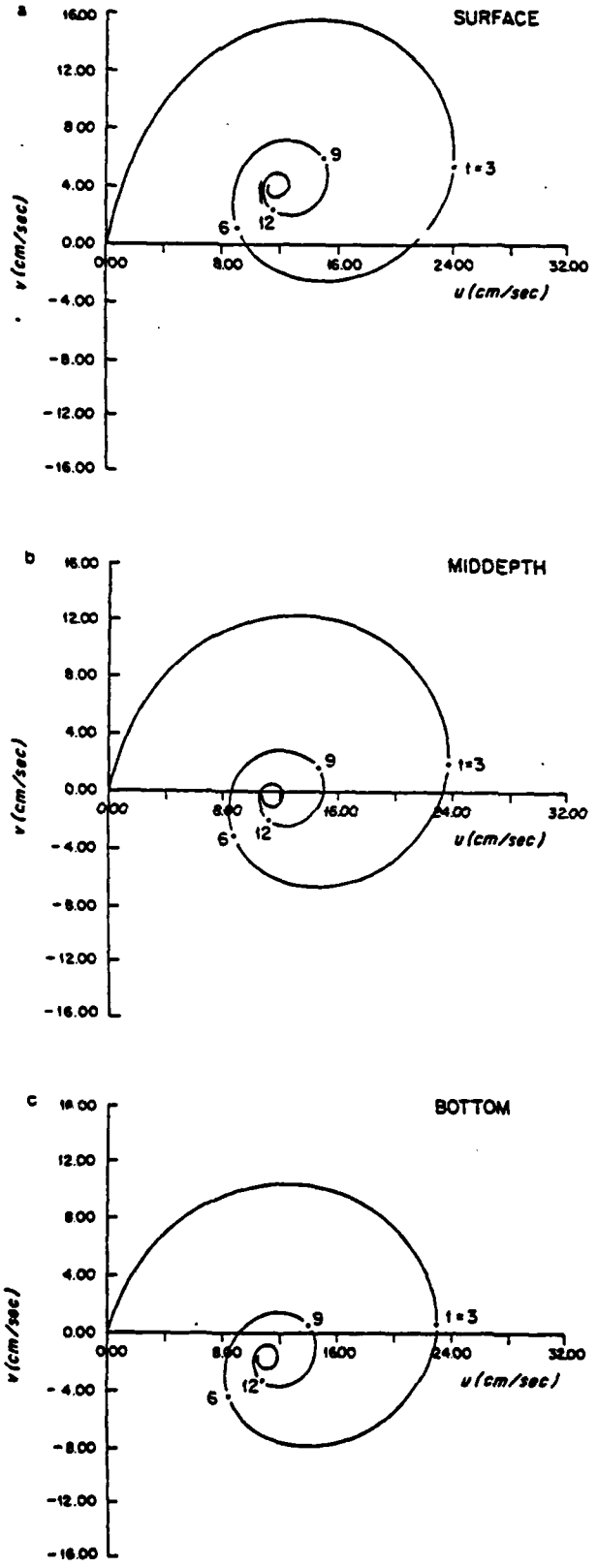

Figure 2.9: Hodographs at (a) surface, (b) middepth, and (c) bottom of mixed layer, with R = 12, c_d = 3 x 10^{-4}, v_* = 1, and initial depth 6m. Fast convergence to steady state values is partly due to the artificial damping associated with the numerical scheme. From Csanady and Shaw (1980).

Section 3
NEAR-INERTIAL INTERNAL WAVES IN AN F-PLANE

When a surface wind field is spatially inhomogeneous, it generates a vertical flow velocity field, known as Ekman pumping, at the base of the surface layer. If the wind field varies in time, then under certain conditions the Ekman pumping couples the surface layer with the inviscid interior. This coupling is achieved through resonances with free internal waves. These free internal waves can then propagate into the deep interior.

In this section we discuss a hierarchy of resonances and models. In Section 3.1 we discuss the resonances that occur between the wind field and the Ekman pumping. We show that a rotational, divergent wind field that oscillates with frequency ω_o has two resonances, at frequencies $(f^2 \pm c^2)^{1/2}$, where c is a damping rate coefficient. This damping results from stresses at the base of the surface layer.

In Section 3.2 we discuss the condition for resonance between the Ekman pumping and internal waves. We show that a wave whose phase speed is equal to the migration speed of the Ekman pumping velocity field satisfies the resonance condition.

We are not interested in the Ekman pumping velocity field per se, but in the vertical shear associated with near-inertial internal waves. In order to describe the locally generated internal wave field in terms of a given

wind field, we combine the concepts developed in Sections 3.1 and 3.2. In Section 3.3 we discuss Krauss' (1976a,b; 1978a,b) model of resonance directly between the surface stress and the internal wave field. We show that if a wind field contains energy in certain horizontal wavenumber ranges, free internal waves are excited.

Finally in Section 3.4 we discuss the propagation of internal waves and their associated vertical structure.

3.1 EKMAN PUMPING IN A VISCOUS SURFACE LAYER

We begin with equations (1.18), simplified here for the case of a homogeneous fluid;

$$u_t - fv = -\partial_z \overline{u'w'}$$

$$v_t + fu = -\partial_z \overline{v'w'}$$

$$u_x + v_y + w_z = 0 \qquad (3.1a\text{-}c)$$

We are concerned primarily with the vertical velocity w_h at the bottom of the surface layer. We integrate (3.1) over the depth h, first by defining

$$(\bar{u},\bar{v},w_h,\tau_o{}^x,\tau_o{}^y) = \int_{-h}^{0} dz(u,v,\partial_z w,\partial_z\overline{u'w'},\partial_z\overline{v'w'}) \qquad (3.2)$$

Here, $\bar{u}$ and $\bar{v}$ have dimensions length^2/time, and

$\underline{\tau}_o = (\tau_o{}^x, \tau_o{}^y)$ is the surface stress vector. Equations (3.1) become

$$\bar{u}_t - f\bar{v} = (\overline{u'w'})_h - \tau_o{}^x$$

$$\bar{v}_t + f\bar{u} = (\overline{v'w'})_h - \tau_o{}^y$$

$$\bar{u}_x + \bar{v}_y = -w_h \ . \qquad (3.3a\text{-}c)$$

We propose a simple bottom drag parameterization for the stresses at depth h;

$$(\overline{u'w'})_h = -c\bar{u}$$

$$(\overline{v'w'})_h = -c\bar{v} \ . \qquad (3.4a,b)$$

As discussed in Section 2.5, if the depth h is chosen to be somewhat greater than the depth $u_*/f = \tau_o{}^{1/2}/f$, then these stresses in (3.4) are very nearly zero. We can combine (3.3a,b) and (3.4) to yield

$$\ddot{\bar{v}} + 2c\dot{\bar{v}} + (c^2+f^2)\bar{v} = f\tau_o{}^x - c\tau_o{}^y - \dot{\tau}_o{}^y \ . \qquad (3.5)$$

Here, the dots indicate partial time derivatives. The importance of this equation lies in the fact that, if $\underline{\tau}_o$ is horizontally homogeneous, then so too is $\bar{v}$. The equation in terms of $\bar{u}$ is analogous. If both $\bar{u}$ and $\bar{v}$ are horizontally homogeneous, then no Ekman pumping occurs; $w_h = 0$ by (3.3c).

We could solve (3.5) and examine its solution, but we are ultimately interested in the internal waves

in the deeper ocean which are driven by w_h. Therefore we take the derivative of (3.5) with respect to y, the derivative of the analogous $\bar{u}$ equation with respect to x, and with the help of (3.3c) we obtain

$$\ddot{w}_h + 2c\dot{w}_h + (c^2+f^2)w_h =$$

$$f\underline{z}\cdot(\nabla x\underline{\tau}_o) + c\nabla\cdot\underline{\tau}_o + \nabla\cdot\dot{\underline{\tau}}_o \quad , \tag{3.6}$$

where $\underline{z}$ is the unit vector in the vertical direction. In the steady state case with no damping, (3.6) simplifies to the well known result for Ekman pumping;

$$w_h = \underline{z}\cdot\nabla x\underline{\tau}_o/f \quad .$$

Because of their similarity, some of the following remarks concerning (3.6) apply also to (3.5).

Equation (3.6) describes the motion of a damped harmonic oscillator. An equation of this type has two solutions; a complementary solution to the homogeneous equation which describes the free, undriven response, and a particular solution to the inhomogeneous equation which describes the driven response.

The complementary solution has the general form

$$w_{hc} = (A\cos ft + B\sin ft)e^{-ct} \quad . \tag{3.7}$$

The natural frequency of the free oscillations is f, and the solution is damped by an exponential envelope. Damped oscillators usually have a natural frequency which is

dependent on the damping constant, but for the special case of (3.5) and (3.6), this dependence exactly cancels!

The particular solution has the form

$$w_{hp} = f^{-1} \sin ft\, e^{-ct} * \left[\nabla\cdot\dot{\underline{I}}_o + c\nabla\cdot\underline{I}_o\right]$$

$$+ \sin ft\, e^{-ct} * \left[\underline{z}\cdot\nabla x\underline{I}_o\right] , \qquad (3.8)$$

where asterisks denote convolution operations with respect to time. This solution is obtained using the method of variation of parameters, along with trigonometric identities. In the case of no damping c is zero, and (3.8) can be simplified using the method of integration by parts;

$$w_{hp} = \sin ft * \underline{z}\cdot(\nabla x\underline{I}_o) - \cos ft * \nabla\cdot\underline{I}_o . \qquad (3.9)$$

We summarize some important results concerning (3.8) and (3.9).

1) The convolution operations imply that the system has a memory of the historical surface stress. In (3.8), the e^{-ct} factor produces a fading memory.

2) The divergence and curl terms indicate that the Ekman suction velocity w_h is produced by horizontal gradients in the surface stress.

3) The Ekman suction velocity is modulated by inertial oscillations, but is not a function of the depth h.

We can look at the particular solution for two selectively chosen surface stresses.

3.1.1 Rotational, Solenoidal Wind Field

We consider only the curl component of the wind stress. When $\underline{\tau}_o$ oscillates with a frequency ω_o, we might express it in the form

$$\underline{\tau}_o = (0, \phi_o(x) \cos\omega_o t) \ . \tag{3.10}$$

The particular solution to (3.6) may be written

$$w_{hp} = \frac{f\, \partial_x \phi_o \cos(\omega_o t - \delta)}{\left[(\omega_o^2 - f^2 - c^2)^2 + 4\omega_o^2 c^2\right]^{1/2}}$$

$$\delta = \tan^{-1}\left(\frac{2\omega_o c}{f^2 + c^2 - \omega_o^2}\right) . \tag{3.11a,b}$$

The damping gives rise to a phase shift δ. The resonant frequency is found by differentiating the amplitude with respect to ω_o, and equating to zero;

$$\omega_r = (f^2 - c^2)^{1/2} \ . \tag{3.12}$$

The effect of damping is to reduce the resonant frequency below the inertial frequency.

It is also interesting to examine the complete solution for w_h in the case of no damping ($c = 0$). If (3.10) describes a surface stress that turns on suddenly at $t = 0$, then appropriate initial conditions are

wh(0) = wh(0) = 0. The complete solution is a combination of complementary and particular solutions, and can be expressed

$$w_h = \frac{2f\,\partial_x\phi_o}{\omega_o^2 - f^2} \sin\frac{(\omega_o + f)t}{2} \sin\frac{(\omega_o - f)t}{2} \quad . \tag{3.13}$$

This solution represents a fast oscillation with frequency $(\omega_o+f)/2$ being modulated by a slow oscillation $(\omega_o-f)/2$. For small time scales $t << (\omega_o-f)^{-1}$, and for a frequency ω_o slightly different than f, an approximation to (3.13) is

$$w_h \simeq (\tfrac{1}{2}\,\partial_x\phi_o)\, t \sin\frac{(\omega_o + f)t}{2} \quad , \tag{3.14}$$

an oscillatory solution whose component grows linearly in time.

3.1.2 Irrotational, Divergent Wind Field

In the case where the curl of the wind field is zero, only the divergence terms in (3.6) remain. We express the wind stress in the form

$$\underline{\tau}_o = (0, \phi_o(y)\cos\omega_o t) \quad . \tag{3.15}$$

$$w_{hp} = \partial_y\phi_o \frac{c\cos(\omega_o t - \delta) + \omega_o \sin(\omega_o t - \delta)}{\left[(\omega_o^2 - f^2 - c^2)^2 + 4\omega_o^2 c^2\right]^{1/2}} \quad . \tag{3.16}$$

The first term, proportional to $\cos(\omega_o t-\delta)$, is analogous to (3.11a), and has a resonant frequency given by (3.12). The second term, with its extra factor ω_o, has a different resonant frequency

$$\omega_r = (f^2+c^2)^{1/2} \quad . \tag{3.17}$$

For a general divergent, rotational wind field, there are two resonant frequencies;

$$\omega_r = (f^2 \pm c^2)^{1/2} , \qquad (3.18)$$

where the plus corresponds to the first two inhomogeneous terms in (3.6), while the minus corresponds to the third inhomogeneous term. So we have two resonant frequencies, one lower and one higher than the inertial frequency. This effect may, in part, be responsible for the two near-inertial peaks resolved by Kundu (1976) in his kinetic energy spectra (see Figure 2.3).

3.2 INTERNAL WAVE RESONANCE WITH EKMAN PUMPING

In Section 3.1 we discussed the surface layer, with particular emphasis on the vertical velocity at its base, known as Ekman pumping. This vertical velocity serves as the driving boundary condition at the top of an interior inviscid layer. We assume here that the depth of the surface layer h is constant in space and time. While this assumption is not generally valid, it does give us a device for decoupling the two layers, and makes the problem tractable.

We start with a set of interior layer equations, identical with (1.18) except that we set the stress terms equal to zero. The interior equations can be combined into a single equation in terms of vertical velocity,

$$\partial^2_t w_{zz} + f^2 w_{zz} + N^2(z)(w_{xx}+w_{yy}) = 0 . \qquad (3.19)$$

The boundary conditions are $w = 0$ at the bottom $z = -H$, and $w = w_h$ given by (3.8) at $z = -h$. If we assume a plane wave solution proportional to $\exp[i(kx+\ell y+mz+\omega t)]$, then we get a relationship

$$\omega^2 = f^2 + N^2(k^2+\ell^2)/m^2 \ . \qquad (3.20)$$

This dispersion relation allows a free internal wave to propagate if its frequency is greater than the inertial frequency f. This means that w_{hc} in (3.7) does not contribute to the production of free internal waves, because w_{hc} represents oscillations purely at the inertial frequency. On the other hand, the second term for w_{hp} in (3.16) does generate free internal waves, since its resonant frequency is greater than f.

Those frequency-wavenumber spectral components of the Ekman pumping that satisfy the internal wave dispersion relation are said to be in resonance with internal waves. We can visualize these resonances in terms of a modal dispersion relation

$$\omega_j^2(k,\ell) = f^2 + (k^2+\ell^2)N^2H^2/(j\pi)^2 \ , \qquad (3.21)$$

where we have replaced m in (3.20) with $j\pi/H$, and have assumed N to be independent of depth. Figure 3.1 is a plot of (3.21) for the first four modes $j = 1, 2, 3, 4$. To be concrete, consider a simple example of an Ekman pumping velocity field, whose spatial form is constant as it migrates with a speed U in the x-direction, and is uniform in the y-direction. Then we could write

$$w_h(x,t) = \int A(k)\exp ik(x-Ut)dk \ , \qquad (3.22)$$

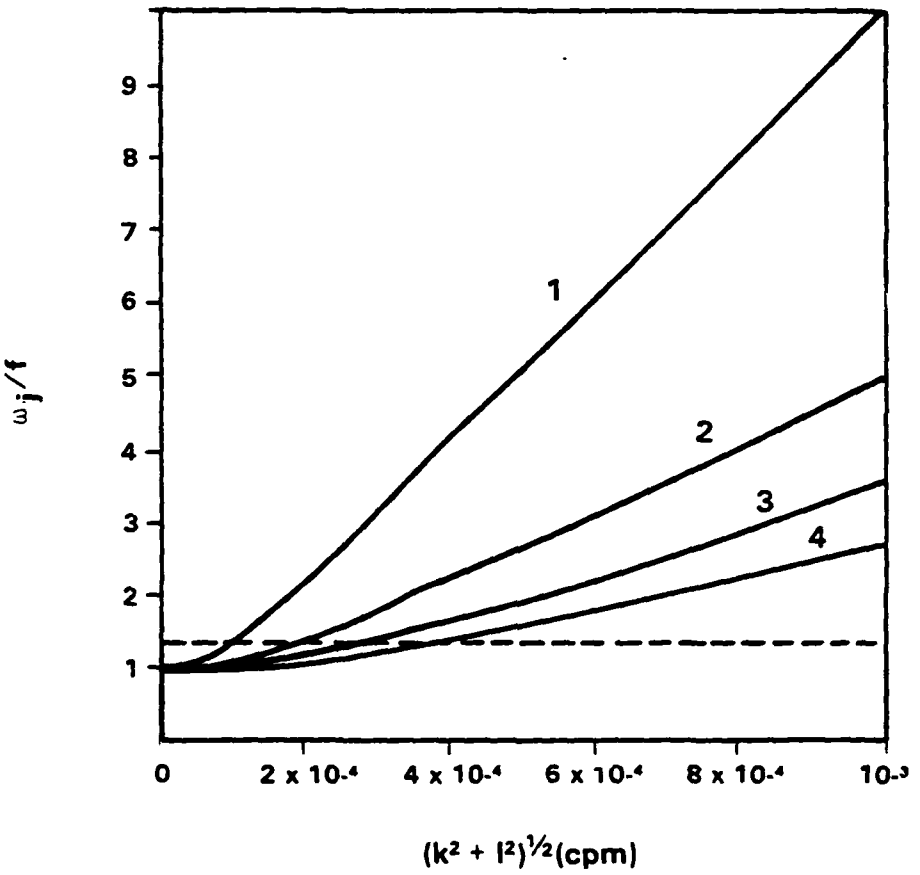

Figure 3.1: Dispersion relation for lowest four modes.

where A(k)dk is the amplitude of the velocity field w_h in a wavenumber band dk centered about a wavenumber k. If A(k) is nonzero at a wavenumber which satisfies (3.15) such that

$$\omega_j(k) = kU \ , \tag{3.23}$$

then an internal wave is excited at the discrete frequency ω_j. Alternatively, we could view the resonance condition (3.23) as a requirement that the phase speed $c = \omega_j/k$ of a resonant wave must be equal to the migration speed U. A front whose length scale is $2\pi/k \sim 10^5$ m must have a migration speed $U \sim 2.2$ m/sec to excite a near-inertial wave of frequency $\omega_j \sim 1.4 \times 10^{-4}$ sec^{-1}.

3.3 INTERNAL WAVE RESONANCE WITH THE WIND FIELD

Miropol'sky (1976) investigated the generation of internal waves using a two-layer model. He derived an expression for the depth dependent horizontal wavenumber spectrum $S(\underline{k},z,t)$ of vertical velocities in terms of the spectral tensor of wind-produced surface stress. For time scales large compared to the integral time scale of the correlation of the wind stress, the expression for $S(\underline{k},z,t)$ simplified to an asymptotic formula. From this formula, Miropol'sky concluded that the resonant growth of internal waves occurs only when the spatial-temporal spectra of the wind stress components contain a set of frequencies and wavenumbers corresponding to the dispersion relations of the free modes of the internal waves.

Although Miropol'sky's solutions are expressed in analytic form, they are not conducive to our obtaining

physical insight. Instead, we review some results from a series of papers by Krauss (1976a,b; 1978a,b; 1981) which also deal with the resonant production of near-inertial frequency internal waves by surface stress. In these papers he presents a model, a method of numerical solution, and a hierarchy of cases, where successive cases have different assumptions about the spatial variability of the wind stress. Krauss (1976a) begins with a set of equations that, when written in a form analogous to (1.18) become

$$u_t + f_o v = -p_x + \partial_z(K\partial_z u) + A\nabla_H^2 u \ ,$$

$$v_t - f_o u = -p_y + \partial_z(K\partial_z v) + A\nabla_H^2 v \ ,$$

$$w_t = -p_z + b \ ,$$

$$b_t + wN^2 = 0 \ ,$$

$$u_x + v_y + w_z = 0 \ . \qquad (3.24a\text{-}e)$$

The following assumptions are made:

1) The horizontal eddy viscosity A is constant.

2) N and K are functions of depth only.

3) The viscous terms are neglected in the vertical momentum and buoyancy equations.

4) Slip is allowed at the sea floor.

We note that the hydrostatic approximation would have been valid, but our discussion in connection with (1.16), (1.17) showed that Krauss' inclusion of the w_t term is inconsistent.

The vertical eddy viscosity $K = (K_1;K_2)$ is taken to be a constant K_1 in an upper 10 m layer, decreases linearly from K_1 to K_2 between 10 m and 15 m, and remains constant at K_2 from 15 m down to the bottom (48 m in the Baltic Sea). The equations were Fourier transformed in time and in the horizontal direction, and were solved numerically in depth.

Krauss expects that resonance should occur at the dispersion lines of free waves. Figure 3.1 shows a representative dispersion relation for modes 1 through 4 in an ocean with a buoyancy frequency profile that is independent of depth. The dashed line represents a slice at a single frequency $\omega > f$. Krauss (1976b) computed equivalent vertical displacements along such a slice, at different depths and for different eddy viscosity distributions $(K_1;K_2)$. Figure 3.2 shows such a computation, for a divergent, irrotational wind field. Krauss defined the equivalent vertical displacement to be the amplitude of the vertical displacement if the particle moved as $w(z)e^{i\omega t}$ during the entire period. The figure caption lists additional details. For small values of viscosity (10;0.1), four distinct modes are produced. As the viscosity increases, the number of modes decreases, as does the resonance amplitudes. When the viscosity is (100,100), the internal waves are entirely suppressed.

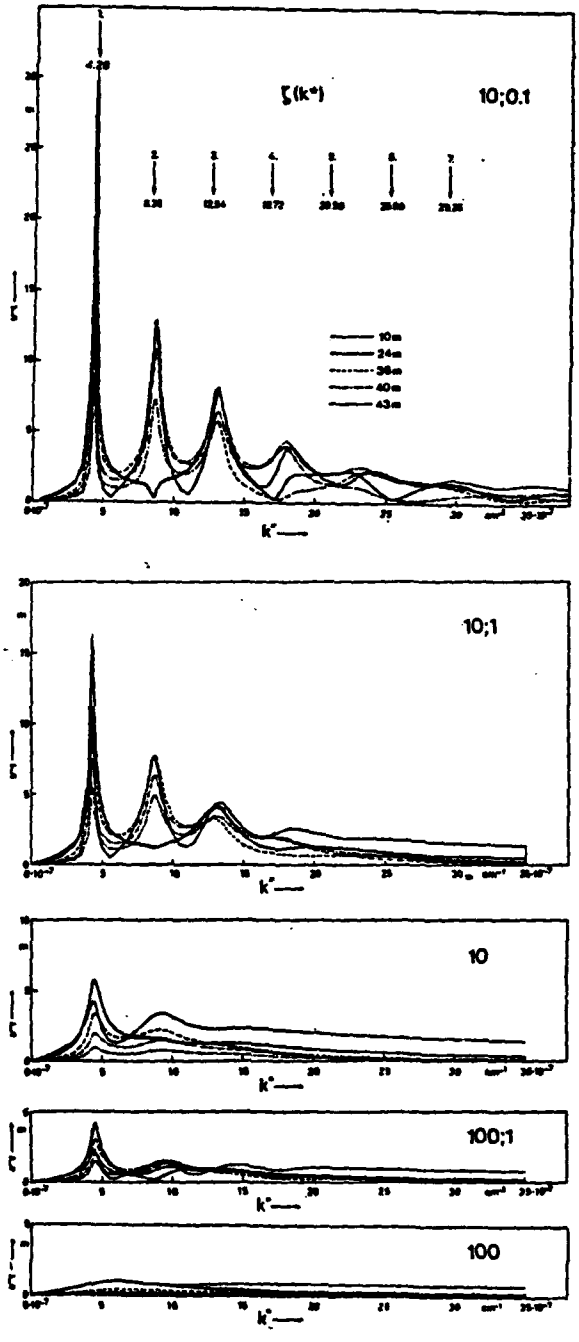

Figure 3.2: Equivalent vertical displacement $\xi(k^*)$ for 10 hr wave period. Number pairs indicate eddy viscosity distribution, single numbers indicate uniform distribution. Arrows at top point to wave numbers of modes in an inviscid sea. From Krauss (1976b).

Before proceeding with an explanation for these results, we refer the reader to Figure 3.3, which shows mean kinetic energy in the surface layer and in the deep layer, for different combinations of viscosity (K_1;K_2). We see that for (10;0.1) and (100;1), the kinetic energy in each of the layers is nearly comparable. As the ratio K_1/K_2 decreases, the resonances broaden, and the deep layer kinetic energy decreases relative to that in the surface layer. In addition, the kinetic energy for both layers in the (100;1) case is an order of magnitude weaker than in the (10:0.1) case.

We explain these results as follows. A certain amount of eddy viscosity is necessary to transfer momentum from the air into the surface layer. If the Ekman depth $\pi(2K_1/f)^{1/2}$ is much less than the surface layer depth, then there is no stress at the base of the surface layer. No significant damping of the Ekman pumping occurs.

The smallest value Krauss used for K_1 was 10 cm^2/sec so the Ekman depth, 12.6 m, is nearly equal to the surface layer depth. Significant damping does occur. From (3.16), the resonance of the second term dominates that of the first term for small values of c. The resonant amplitudes of the first and second terms are $(2f)^{-1}$ and $(2c)^{-1}$, respectively. As c increases, the resonant amplitude of the second term decreases, and the halfwidths of both terms broaden. This effect helps to explain the resonance broadening in Figures 3.2 as 3.3 as K_1 increases from 10 to 100 cm^2/sec.

As viscosity increases in the interior, momentum is allowed to diffuse from the surface layer into the

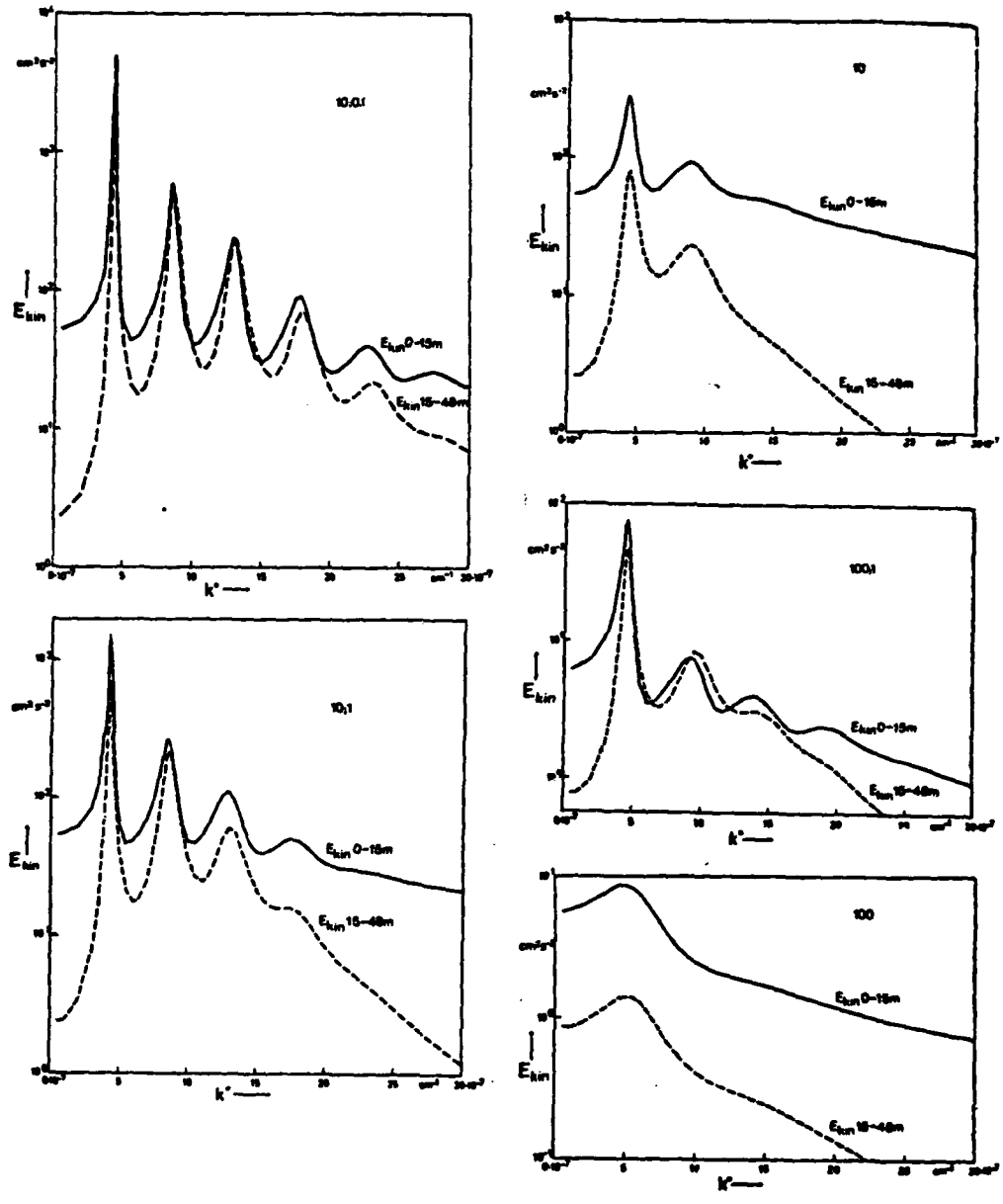

Figure 3.3: Mean kinetic energy of the surface layer (0 to 15m) and the deep layer (15 to 48m). From Krauss (1976b).

interior at a faster rate, resulting in increased damping of the Ekman pumping. From Figure 3.2a, we see that the resonant amplitudes are nearly inversely proportional to the mode number. Therefore as the interior viscosity K_2 increases, the reduction in resonant amplitudes in the interior is nearly independent of mode number.

Krauss' (1978a) interpretation of these figures is of value. We can think of these diagrams as being response functions $H_q(k,\omega)$ such that

$$q(k,\omega) = H_q(k,\omega)\tau_o(k,\omega) ,$$

for any physical variable q. The resonance peaks correspond to free internal waves. Typical gain factors range from 2 to 10. Surface stress components whose wavenumbers fall outside the resonant peaks generate forced, or trapped internal waves, in the sense that they are not free to propagate away from their local source. Stress components whose wavenumbers fall in the vicinity of resonant peaks generate freely propagating internal waves. This is the subject of the next section.

3.4 PROPAGATION OF NEAR-INERTIAL FREQUENCY INTERNAL WAVES

3.4.1 WKB Solution

We wish to analyze the propagation of low frequency internal waves. We start with an Ekman pumping vertical velocity at the base of the surface layer as the source of internal waves, and examine their propagation

downward into the interior. We assume that the vertical velocity at $z = -h$ is of the form:

$$w(z = -h) = W_h(x,t)\exp[i(kx - \omega t)], \qquad (3.25)$$

where the amplitude $W_h(x,t)$ is a weak function of x and t; $\partial_x W_h/W_h$ and $\partial_t W_h/W_h$ are much less than k and ω, respectively.

The equation of motion from (3.19) is

$$\partial_z^2(\partial_t^2 + f^2)w + N^2(z)(\partial_x^2 + \partial_y^2)w = 0 \qquad (3.26)$$

With no loss of generality, we let the horizontal component of propagation be in the x-direction. Then we can assume a solution for w of the form

$$w(x,z,t) = w_o(x,z,t)\exp\left[iS(x,z,t)\right] \quad . \qquad (3.27)$$

S(x,z,t) is a phase function which varies much more rapidly with x, z, and t than the amplitude function w_o. We let

$$\partial_x S = k \quad ,$$
$$\partial_z S = m \quad ,$$
$$\partial_t S = -\omega \quad , \qquad (3.28a\text{-}c)$$

so that (3.16) becomes

$$\partial_z^2 w_o + m^2 w_o = 0,$$

$$m^2(z) = k^2N^2(z)/(\omega^2 - f^2) \quad . \qquad (3.29a,b)$$

In order that m be real valued, we require $\omega > f$. The terms k and ω are the horizontal wavenumber and frequency, and m(z) acts as a local vertical wavenumber.

If N(z) is a smoothly varying function, that is $N'(z)/N(z) \ll m(z)$, then the WKB approximate solution is appropriate;

$$w = A\, m(z)^{-1/2} \exp\left[i\left(kx \pm \int m\,dz - \omega t\right)\right]. \qquad (3.30)$$

Here, the integration limits are -h and z, and A is a constant to be determined by the boundary condition at z = -h. For concreteness, we set

$$A = W_h\, m_h^{1/2}, \qquad (3.31)$$

where $m_h = m(z = -h)$, so that (3.30) agrees with the boundary condition--and since we are concerned with only downward propagation we retain only the lower minus sign in (3.30). Then the real valued solutions for u, v, and w (see Kundu; 1976) are

$$w = W_h \left(\frac{m_h}{m}\right)^{1/2} \cos\phi \quad ,$$

$$u = W_h \frac{(m_h m)^{1/2}}{k} \cos\phi \quad ,$$

$$v = W_h \frac{f}{\omega} \frac{(m_h m)^{1/2}}{k} \sin\phi \quad , \qquad (3.32a\text{-}d)$$

$$\phi = kx - \int m\,dz - \omega t \quad .$$

3.4.2 Energy Propagation

Energy propagates downward, away from points on the plane z = -h, along characteristic curves. The propagation proceeds at the local group velocity $\underline{c}_g$, given by $\underline{c}_g = (\partial\omega/\partial k, \partial\omega/\partial m)$. Using the characteristic equation (3.19b), we compute the group velocity to be

$$\underline{c}_g = \frac{\omega^2 - f^2}{\omega k} \left(1, -(\omega^2-f^2)^{1/2}/N(z)\right) \quad . \qquad (3.33)$$

For near inertial frequencies, $\omega - f << f$ holds, and the magnitude of the group velocity is approximately

$$|\underline{c}_g| \simeq 2(\omega-f)/k \quad , \qquad (3.34)$$

and if $N(z) >> f$, then the angle θ of the group velocity vector with respect to the horizontal is very small:

$$\theta \simeq \tan^{-1}\left(\frac{\sqrt{2(\omega-f)f}}{N(z)}\right) \simeq \frac{\sqrt{2(\omega-f)f}}{N(z)} \quad . \qquad (3.35)$$

Pollard's (1980) analysis of current meter records give us some insight into the propagation of near-inertial internal waves. Figure 3.4 illustrates horizontal and vertical coherences, and vertical phase differences among three moorings, separated horizontally by about 50 km. Figure 3.4c shows statistically that significant values of vertical coherence correspond to upward phase propagation; phase differences all lie between 20° and 70°. The vertical component of group velocity is therefore directed downward,

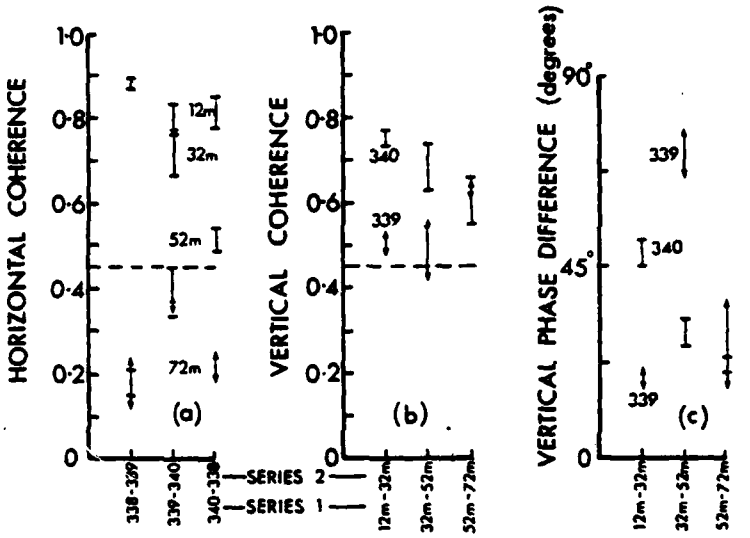

Figure 3.4: Coherence and phase of frequencies between $(20.89)^{-1}$ and $(16.25)^{-1}$ cph. For each pair of vector time series, four values of coherence and phase can be calculated (Webster, 1968). Each vertical bar joins the minimum and maximum of the four values. Horizontal coherence values (a) are given for pairs of records at the same depth on different moorings. Vertical coherence (b) and phase (c) are given for pairs of records on the same mooring 20m apart. Phases are modified by $\pm$ 90° (cf. Webster, 1968) to give the angle by which the second series leads the first series. The 95% limit for the coherence is 0.45. From Pollard (1980).

and the inertial oscillations at 32, 52, and 72m are wind-forced oscillations dispersing away from the surface. From measurements of horizontal and vertical phase differences, Pollard estimated the group velocity to be on the order of

$$\underline{c}_g \sim (1\text{-}20 \text{ km/day}, 0.03\text{-}3 \text{ m/day}),$$

and suggests these small values are responsible for the rapid loss of horizontal coherence with increasing depth in Figure 3.4a. Using the maximum group velocity estimates, it takes 6-7 days for near-inertial energy to propagate 20m vertically, and 3-4 days to travel from one mooring to another. During these several-day periods and over tens of kilometers the variability in the upper ocean reduces the coherence of the inertial motions. The group velocity is sensitive to horizontal variations in stratification, and coherence may be destroyed by a number of processes, including Kelvin Helmholtz instability, turbulence, and mean horizontal as well as vertical shear.

3.4.3 Vertical Shear

Equations (3.32b,c) describe a horizontal velocity vector that, at any given point in space, rotates in a clockwise ellipse in time. The major axis is in the direction of propagation, and the minor axis is smaller by the ratio f/ω.

The horizontal velocity vector turns as a function of depth. Looking down, the turning is clockwise with increasing depth for upward propagation, and counterclockwise for downward propagation. Kundu (1976) computed the

turning rate, but we suspect there is a misprint in his text. The corrected computation follows below. Define ϕ as the angle between the horizontal velocity vector and the direction of horizontal propagation, the x-axis. Then from (3.32b,c)

$$\tan\phi = \frac{v}{u} = \frac{f}{\omega} \tan(kx - \int m dz - \omega t) \quad . \tag{3.36}$$

The turning rate can be written

$$\frac{d\phi}{dz} = -m \frac{f}{\omega} \left[\frac{1 + \tan^2(kx - \omega t - \int m dz)}{1 + (f/\omega)^2 \tan^2(kx - \omega t - \int m dz)} \right] \quad . \tag{3.37}$$

With the approximation $\omega \simeq f$, (3.37) becomes

$$\frac{d\phi}{dz} \simeq -m(z) \quad , \tag{3.38}$$

which simply states that the velocity vector turns by about 360° in a distance equal to the vertical wavelength.

We can also compute the vertical shear;

$$S^2 = u_z^2 + v_z^2 \simeq \frac{w_h^2 \, m_h}{k^2} (m^3 + m_z^2/4m) \quad . \tag{3.39}$$

From the WKB approximation $N_z/N << m$, we are justified in neglecting the second term in parentheses in (3.39). Then combining (3.29b) and (3.39) gives

$$S^2(z) \simeq \frac{W_h^2 \, m_h k N^3(z)}{(\omega^2 - f^2)^{3/2}} \quad . \tag{3.40}$$

Here we have derived a standard WKB result, that S^2 is proportional to N^3. We can interpret these results in a simple manner. From (3.22b), we could express the amplitude of the horizontal current as

$$|U| = W_h (m_h m)^{1/2} \, k^{-1} \quad , \tag{3.41}$$

and the shear becomes

$$S(z) = |U(z)| \, m(z) \quad . \tag{3.42}$$

In the case of a uniformly stratified ocean, the vertical wavelength λ_v is $2\pi/m$, and (3.32) might be written

$$S = 2\pi |U| / \lambda_v \quad . \tag{3.43}$$

We emphasize that these results apply for a monochromatic internal wave that would accompany an ideal sinusoidal form of Ekman suction (3.15), hence an ideal sinusoidal surface stress.

Section 4
SUMMARY AND FUTURE RESEARCH

Most of the research to date deals with the resonant excitation of internal waves by wind forcing. The emphasis has been on the growth rate of resonant vertical modes, where the internal wave field responds to a steady state wind field. A steady state wind field, though, is not a realistic model of the atmosphere. A wind forcing event with a horizontal wavenumber component k and propagation speed U may be in resonance with the internal wave field for a short while. However, if U is not constant, the response will quickly slip out of that resonance, and perhaps into a different one.

For these reasons, it appears that near-inertial frequency internal waves are transient responses to variable wind forcing. An important problem that should be addressed is the response due to wind events that propagate with variable speed, or whose structure or length scales evolve in time. A particular aspect of this problem would be to determine the degree of statistical stationarity required of a wind field, in order to elicit a resonant response.

To be able to study the transient response of the internal wave field, we are developing a numerical model of a wind-forced, viscous, stratified ocean. The model equations are similar to those of Krauss, but the method of solution is different. By employing a finite difference scheme which marches the solutions forward in time, it is possible to study the generation of near-inertial motions

and shear. The model does not impose severe limitations on the functional form of the wind field, and does not require that it be periodic in time. Details concerning the model and results will be given in Rubenstein (1981).

APPENDIX A

We solve the equation

$$U_t + if\,U - KU_{zz} = Q(z,t) + U_o(z)\delta(t) \qquad (A.1)$$

for a complex source distribution of momentum $Q(z,t)$ and an initial complex velocity $U_o = U(z,0)$. With a horizontally homogeneous source distribution, we let $Q = 2\tau_o(t)\,\delta(z)$, where the factor of two enters because we have extended our domain, in a virtual sense, above the plane $z = 0$. We then write

$$U_t + if\,U - KU_{zz} = 2\tau_o(t)\delta(z) \quad . \qquad (A.2)$$

We apply a Laplace transform operation to (A.2) with respect to t:

$$sU(z,s) - U_o(z) + ifU(z,s) - KU_{zz}(z,s) = 2\tau_o(s)\delta(z) \qquad (A.3)$$

Next we take the inverse Fourier transform of (A.3) with respect to z;

$$sU(\beta,s) + (if + 4\pi^2\beta^2 K)U(\beta,s) = U_o(\beta) + 2\tau_o(s) \qquad (A.4)$$

We can solve for $U(\beta,s)$

$$U(\beta,s) = \left[s + (if + 4\pi^2\beta^2 K)\right]^{-1}\left[U_o(\beta) + 2\tau_o(s)\right] \quad . \qquad (A.5)$$

and take the inverse Laplace transform to get

$$U(\beta,t) = \exp\left[-(if + 4\pi^2\beta^2K)t\right] U_o(\beta)$$
$$+ \left\{\exp\left[-(if + 4\pi^2\beta^2K)t\right]\right\} \underset{(t)}{*} 2\tau_o(t) \quad . \tag{A.6}$$

Here the asterisk indicates the operation of convolution with respect to t. Now we take the Fourier transform of (A.6) with respect to z; we use the fact that the Fourier transform of $\exp(-\pi a\beta^2)$ is $a^{-1/2}\exp(-\pi z^2/a)$ and the convolution theorem to yield

$$U(z,t) = e^{-ift}(4\pi Kt)^{-1/2}\left[\exp(-z^2/4Kt)\right] \underset{(z)}{*} U_o(z)$$
$$+\left[e^{-ift}(4\pi Kt)^{-1/2}\exp(-z^2/4Kt)\right] \underset{(t)}{*} 2\tau_o(t) \tag{A.7}$$

In the special case of a steady state situation, we set $U_t = 0$ in (A.2) and Fourier transform with respect to z;

$$U(\beta) = \frac{2\tau_o}{if + 4\pi^2\beta^2K} \quad . \tag{A.8}$$

We let $a^2 = if/K$, so that (A.8) may be written

$$U(\beta) = \frac{\tau_o}{Ka}\frac{2a}{a^2 + (2\pi\beta)^2} \quad . \tag{A.9}$$

The inverse Fourier transform of (A.9) is

$$U(z) = \frac{\tau_o e^{-i\pi/4}}{(fK)^{1/2}}\exp\left[-(1 + i)(f/2K)^{1/2}\,|z|\right] \quad . \tag{A.10}$$

This result is the well known Ekman spiral. At the surface, with $z = 0$, the phase $e^{-i\pi/4}$ indicates that the current is 45^{o} to the right of the wind stress.

Parenthetically, it is helpful here to define the convolutions in (A.7). With the appropriate symmetry of $U_o(z)$, the convolution with respect to z is defined by

$$f(z) * U_o(z) = \int_{-\infty}^{\infty} f(y)U_o(z-y)dy. \qquad (A.11)$$

Also, the convolution with respect to t is defined by

$$f(t) * \tau_o(t) = \int_{0}^{t} f(y)\tau_o(t-y)dy. \qquad (A.12)$$

References

Csanady, G. T., 1978: Turbulent interface layers, J. of Geophys. Res., 83, 2329-2342.

Csanady, G. T., and P. T. Shaw, 1980: The evolution of a turbulent Ekman layer. J. of Geophys. Res., 85, 1537-1547.

Ekman, V. W., 1905: On the influence of the earth's rotation on ocean currents. Ark. Mat. Astr., Fys., 2, 11.

Fu, Lee-Lueng, 1980: Observations and models of inertial waves in the deep ocean. Doctoral Dissertation, Woods Hole Oceanographic Institution/Massachusetts Institute of Technology, WHOI-80-11.

Gonella, J. 1971: A local study of inertial oscillations in the upper layers of the ocean. Deep-Sea Res., 18, 775-788.

Krauss, W., 1976a: On currents, internal and inertial waves in a stratified ocean due to variable winds, Part 1. Deutsche Hydro. Zeitsch., 29, 87-96.

Krauss, W., 1976b: On currents, internal and inertial waves in a stratified ocean due to variable winds, Part 2. Deutsch Hydro. Zeitsch., 29, 119-135.

Krauss, W., 1978a: The response of a stratified viscous sea to moving meteorological fronts and squall lines. Deutsche Hydro. Zeitsch., 31, 16-30.

Krauss, W., 1978b: On the energy of the wind stress required to produce internal and inertial waves. Deutsche Hydro. Zeitsch., 31, 31-49.

Krauss, W., 1981: The erosion of the thermocline. J. Phys. Oceanogr., 11, 415-433.

Kundu, P. K., 1976: An analysis of inertial oscillations near Oregon coast. J. Phys. Oceanogr., 6, 879-893.

Madsen, O. S., 1977: A realistic model of the wind-induced Ekman boundary layer. J. Phys. Oceanogr., 7, 248-255.

References (Continued)

Miropol'skiy, Yu. Z., 1976: Generation of internal waves in the ocean by the wind field. Oceanology, 15, 266-270.

Newman, F. C., 1981: Interpretation of Analysis of Shear from Ocean Current Meters, Science Applications, Inc., Ocean Physics Division, McLean, VA. to be submitted.

Pollard, R. T., R. B. Rhines, and R. O. R. Y. Thompson, 1973: The deepening of the wind-mixed layer. Geophysical Fluid Dynamics, 3, 381-404.

Pollard, R. T., 1980: Properties of near-surface inertial oscillations. J. Phys. Oceanogr., 10, 385-398.

Rubenstein, D. M., 1981: A Dynamical Model of Wind-Induced Near-Inertial Motions, Science Applications, Inc., Ocean Physics Division, McLean, VA. To be submitted.

Rubenstein, D. M. and F. C. Newman, 1981: Analysis and Interpretation of Shear from Ocean Current Meters, Science Applications, Inc., Ocean Physics Division, McLean, VA.

Webster, F., 1968: Observations of inertial-period motions in the deep-sea. Rev. of Geophys., 6, 473-490.